AIP | The Journal of Chemical Physics

B27 −: Appearance of the smallest planar boron cluster containing a hexagonal vacancy

Wei-Li Li, Rhitankar Pal, Zachary A. Piazza, Xiao Cheng Zeng, and Lai-Sheng Wang

Citation: The Journal of Chemical Physics **142**, 204305 (2015); doi: 10.1063/1.4921732
View online: http://dx.doi.org/10.1063/1.4921732
View Table of Contents: http://scitation.aip.org/content/aip/journal/jcp/142/20?ver=pdfcov
Published by the AIP Publishing

B_{27}^-: Appearance of the smallest planar boron cluster containing a hexagonal vacancy

Wei-Li Li,[1,a)] Rhitankar Pal,[2,a)] Zachary A. Piazza,[1] Xiao Cheng Zeng,[2,b)] and Lai-Sheng Wang[1,b)]
[1]*Department of Chemistry, Brown University, Providence, Rhode Island 02912, USA*
[2]*Department of Chemistry, University of Nebraska-Lincoln, Lincoln, Nebraska 68588, USA*

(Received 16 April 2015; accepted 14 May 2015; published online 27 May 2015)

Photoelectron spectroscopy and *ab initio* calculations have been carried out to probe the structures and chemical bonding of the B_{27}^- cluster. Comparison between the experimental spectrum and the theoretical results reveals a two-dimensional (2D) global minimum with a triangular lattice containing a tetragonal defect (**I**) and two low-lying 2D isomers (**II** and **III**), each with a *hexagonal* vacancy. All three 2D isomers have 16 peripheral boron atoms and 11 inner boron atoms. Isomer **I** is shown to be mainly responsible for the observed photoelectron spectrum with isomers **II** and **III** as minor contributors. Chemical bonding analyses of these three isomers show that they all feature 16 localized peripheral B–B σ-bonds. Additionally, isomer **I** possesses 16 delocalized σ bonds and nine delocalized π bonds, while isomers **II** and **III** each contain 17 delocalized σ bonds and eight delocalized π bonds. It is found that the hexagonal vacancy is associated generally with an increase of delocalized σ bonds at the expense of delocalized π bonds in 2D boron clusters. The hexagonal vacancy, characteristic of borophenes, is found to be a general structural feature for mid-sized boron clusters. The current study shows that B_{27}^- is the first boron cluster, where a hexagonal vacancy appears among the low-lying isomers accessible experimentally. © *2015 AIP Publishing LLC.* [http://dx.doi.org/10.1063/1.4921732]

I. INTRODUCTION

Photoelectron spectroscopy (PES) and *ab initio* calculations have uncovered a world of planar boron clusters (B_n^-) at least up to $n = 25$,[1–14] in sharp contrast with the three-dimensional (3D) cage building blocks in bulk boron.[15–17] Positively charged boron clusters were observed in an ion mobility experiment and were found to be planar up to 16 atoms.[18] Although neutral boron clusters were computationally suggested to have a 3D double-ring structure at the size of $n = 20$,[4,5] a later UV-IR experiment did not detect such double-ring structure.[19] Boron clusters in this size range ($n \leq 25$) consist of triangular lattices with tetragonal or pentagonal vacancies. These vacancies together with delocalized bonding give rise to interesting fluxionality for the planar boron clusters.[20–24] However, there seems to be a tendency for larger vacancy sizes as the cluster size increases.[25] The two-dimensional (2D) structures of boron clusters at such large sizes are interesting, suggesting the possibilities of novel 2D boron-based nanostructures. In fact, since the discovery of carbon nanotubes and graphene, computational investigations have been carried out to examine the possibility of boron nanotubes and extended atom-thin boron nanosheet.[26–30] Early theoretical calculations suggested that graphene-like boron nanosheets are unstable. Instead, boron was found to prefer buckled triangular lattice from several computational studies.[26–29] More recent calculations have shown that perfect planar boron nanosheets could be achieved by creating hexagonal vacancies in a triangular lattice with different vacancy densities and patterns.[31–37] However, such nanostructures have yet to be realized experimentally.

A major breakthrough in the study of boron clusters took place recently with the observation of a special PES spectrum of B_{36}^-, which was found to exhibit a large energy gap and an unusually low electron binding energy.[38] Global minimum searches led to the discovery of a 2D structure with a central hexagonal hole. Neutral B_{36} possesses a perfect C_{6v} structure and can be viewed as an embryo of the extended 2D boron sheet with hexagonal vacancies, providing the first indirect experimental evidence of the viability of such boron nanostructures. A name "borophene" was coined to designate such atomic-thin boron nanosheets.[38] A subsequent joint PES and *ab initio* study found that the B_{35}^- cluster has a twin-hexagonal vacancy, simply by removing one boron atom from the interior of B_{36}^-.[39] More importantly, the B_{35}^- cluster with the twin-hexagonal vacancy is shown to be an even more flexible structural motif for borophenes with different hexagonal vacancy densities and patterns, providing further experimental evidence for the viability of borophenes. More recently, the B_{40}^- cluster was found to possess two nearly degenerate isomers: a planar one containing a double-hexagonal vacancy and a 3D hollow-cage structure containing two hexagons and four heptagons. The B_{40}^- cage isomer was the first all-boron fullerene ever observed experimentally.[40] The neutral B_{40} cage was found to be overwhelmingly the global minimum with a large HOMO-LUMO gap and it is named "borospherene."[40] Very recently, the global minimum of the B_{39}^- cluster is found to consist

a)W.-L. Li and R. Pal contributed equally to this work.
b)Authors to whom correspondence should be addressed. Electronic addresses: xzeng1@unl.edu and lai-sheng_wang@brown.edu.

of two nearly degenerate axially chiral structures related to that of the B_{40} cage, and thus B_{39}^- is the first axially chiral borospherene.[41] In the smaller size range, the B_{30}^- cluster was found to contain a hexagonal vacancy, which is the first inherently chiral boron cluster to be characterized.[42] The hexagonal vacancy seems to be a defining feature in 2D boron clusters in the size range between 30 and 40 atoms. Hence, a question arises: what is the smallest boron cluster with a hexagonal vacancy?

Higher-lying 2D isomers with hexagonal holes were already seen in B_{21}^-.[12] Such hexagon-containing 2D isomers become more stable relative to the global minimum as the cluster size increases. Thus, we expect that B_n^- clusters with a hexagonal hole should be the global minimum between B_{26}^- and B_{30}^-. Here, we report a joint PES and computational study of B_{27}^-. The global minimum is found to be a 2D structure (isomer **I**) featuring a tetragonal hole. A low-lying isomer that contains a hexagonal hole (isomer **II**) is found to be only 2 kcal/mol higher in energy, and it is energetically accessible under the experimental condition and is observed to contribute to the experimental PE spectrum. Isomer **I** is related to the structure of B_{25}^- and isomer **II** is related to the structure of B_{30}^-. Thus, the B_{27}^- cluster can be considered as the turning point for the appearance of 2D boron clusters with a hexagonal vacancy.

II. EXPERIMENTAL AND COMPUTATIONAL METHODS

A. Photoelectron spectroscopy

The experiment was carried out using a magnetic-bottle PES apparatus equipped with a laser vaporization cluster source, details of which can be found elsewhere.[43] Briefly, negatively charged boron clusters were produced by laser vaporization of a hot-pressed ^{10}B disk target (96% isotopically enriched). Clusters formed in the nozzle were entrained in a He carrier gas containing 5% Ar and underwent a supersonic expansion, forming a collimated and cold cluster beam. The cluster temperature was controlled to some degree by the resident time in the nozzle and the supersonic expansion.[44,45] Negatively charged clusters were extracted from the cluster beam and analyzed with a time-of-flight mass spectrometer. The B_{27}^- cluster of interest was mass-selected and decelerated before photodetachment. For the current study, the 193 nm (6.424 eV) radiation from an ArF excimer laser was used. Photoelectrons were collected at nearly 100% efficiency by a magnetic bottle and analyzed in a 3.5 m long electron flight tube. The PE spectrum was calibrated using Bi^- and the electron kinetic energy (E_k) resolution of the apparatus was $\Delta E_k/E_k \sim 2.5\%$, i.e., ~25 meV for 1 eV electrons.

B. Global minimum searches and computational methods

Global minimum searches were performed using both the Cartesian walking (CW)[12] and the basin-hopping (BH) algorithms.[46] The initial structures generated by CW method were optimized using the Perdew, Burke, Ernzerhof exchange correlation functional (PBE0)[47] and the 3-21G basis set.[48] The initial structures generated by BH were optimized using the TPSSh functional[49] and the 3-21G basis set. The isomers within 40 kcal/mol were then refined at the PBE0 and the hybrid exchange functional of Tao, Perdew, Staroverov, and Scuseria (TPSSh) with the larger 6-311+g* basis set,[50,51] followed by single-point calculations using a more expensive basis set of 6-311+g(2df). Frequency analyses at DFT/6-311+g(2df) were conducted to ensure that each structure is a true minimum on its potential energy surface. Zero-point energy (ZPE) corrections were made at the corresponding level of theory for each DFT method.

For comparison with the experimental spectrum, we computed the vertical detachment energies (VDEs) of each electronic state at the DFT/6-311+g* level of theory. The first VDE was calculated as the energy difference between the anion and the neutral at the anionic geometry. The higher VDEs were approximated by adding time-dependent DFT vertical excitation energies to the first VDE. The adiabatic detachment energy (ADE) was calculated as the energy difference of the anion and the neutral at its optimized structure. We used the adaptive natural density partitioning (AdNDP) method to analyze the chemical bonding in B_{27}^-.[52] To prevent the mixing of σ and π orbitals of quasi-planar structures, we artificially flattened the 2D structures for the AdNDP analyses, which does not change the number of the canonical molecular orbitals (CMOs) and their nodal characters compared to the original structure.[12,13] The AdNDP analyses were done at the PBE0/3-21g level of theory.

All calculations with the PBE0, TPSSh, and coupled-cluster approach with single and double and perturbative triple excitations (CCSD(T)) methods were performed with the Gaussian09 program.[53] Structural and chemical bonding visualizations were performed using Molekel 5.4.0.8[54] and GaussView 5.0,[55] respectively.

III. EXPERIMENTAL RESULTS

The 193 nm PE spectrum of B_{27}^- is shown in Figure 1. The photodetachment features are labeled with letters, which correspond to detachment transitions from the anion ground state to the neutral ground state (X) and excited states (A, B, . . .). All the VDEs are summarized in Table I, where they are compared with the calculated VDEs.

The B_{27}^- spectrum exhibits congested, yet well-defined features. The ground state transition (X) has a VDE of 4.09 eV.

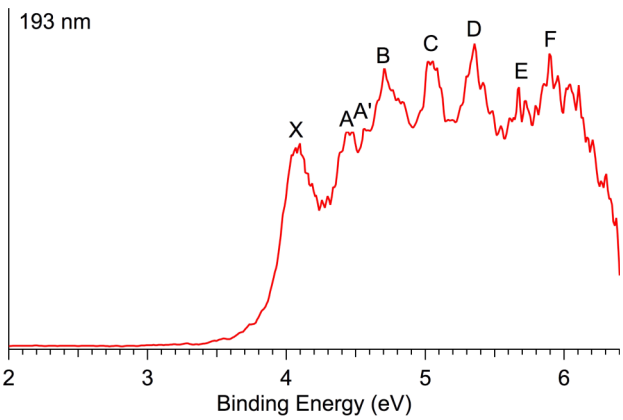

FIG. 1. Experimental photoelectron spectrum of B_{27}^- at 193 nm (6.424 eV).

TABLE I. Observed VDEs for B_{27}^- and comparison with calculated VDEs for isomers **I–III** at two levels of theory. All energies are in eV.

	VDE (expt.)[a]	Final state and electronic configuration	VDE (theo.) PBE0[b]	VDE (theo.) TPSSh[c]
		Isomer **I** (C_1, ^1A)		
X	4.09(6)	$^2A\ldots(33a)^2(34a)^2(35a)^2(36a)^2(37a)^2(38a)^2(39a)^2(40a)^2(41a)^1$	3.98	3.89
A	4.44(6)	$^2A\ldots(33a)^2(34a)^2(35a)^2(36a)^2(37a)^2(38a)^2(39a)^2(40a)^1(41a)^2$	4.46	4.33
B	4.71(6)	$^2A\ldots(33a)^2(34a)^2(35a)^2(36a)^2(37a)^2(38a)^2(39a)^1(40a)^2(41a)^2$	4.71	4.53
C	5.05(6)	$^2A\ldots(33a)^2(34a)^2(35a)^2(36a)^2(37a)^2(38a)^1(39a)^2(40a)^2(41a)^2$	5.07	4.87
D	5.35(5)	$^2A\ldots(33a)^2(34a)^2(35a)^2(36a)^2(37a)^1(38a)^2(39a)^2(40a)^2(41a)^2$	5.32	5.12
E	5.68(8)	$^2A\ldots(33a)^2(34a)^2(35a)^2(36a)^1(37a)^2(38a)^2(39a)^2(40a)^2(41a)^2$	5.75	5.51
F	5.89(6)	$^2A\ldots(33a)^2(34a)^2(35a)^1(36a)^2(37a)^2(38a)^2(39a)^2(40a)^2(41a)^2$	6.11	[d]
		$^2A\ldots(33a)^2(34a)^1(35a)^2(36a)^2(37a)^2(38a)^2(39a)^2(40a)^2(41a)^2$	6.38	6.27
		Isomer **II** (C_1, $^1A_1$)		
		$^2A\ldots(33a)^2(34a)^2(35a)^2(36a)^2(37a)^2(38a)^2(39a)^2(40a)^2(41a)^1$	4.14	4.14
		$^2A\ldots(33a)^2(34a)^2(35a)^2(36a)^2(37a)^2(38a)^2(39a)^2(40a)^1(41a)^2$	4.39	4.42
		$^2A\ldots(33a)^2(34a)^2(35a)^2(36a)^2(37a)^2(38a)^2(39a)^1(40a)^2(41a)^2$	4.57	4.58
A′	4.56(8)	$^2A\ldots(33a)^2(34a)^2(35a)^2(36a)^2(37a)^2(38a)^1(39a)^2(40a)^2(41a)^2$	4.93	4.96
		$^2A\ldots(33a)^2(34a)^2(35a)^2(36a)^2(37a)^1(38a)^2(39a)^2(40a)^2(41a)^2$	5.35	5.34
		$^2A\ldots(33a)^2(34a)^2(35a)^2(36a)^1(37a)^2(38a)^2(39a)^2(40a)^2(41a)^2$	5.75	5.56
		$^2A\ldots(33a)^2(34a)^2(35a)^1(36a)^2(37a)^2(38a)^2(39a)^2(40a)^2(41a)^2$	5.84	[d]
		Isomer **III** (C_1, $^1A_1$)		
		$^2A\ldots(33a)^2(34a)^2(35a)^2(36a)^2(37a)^2(38a)^2(39a)^2(40a)^2(41a)^1$	4.02	3.89
		$^2A\ldots(33a)^2(34a)^2(35a)^2(36a)^2(37a)^2(38a)^2(39a)^2(40a)^1(41a)^2$	4.29	4.22
		$^2A\ldots(33a)^2(34a)^2(35a)^2(36a)^2(37a)^2(38a)^2(39a)^1(40a)^2(41a)^2$	4.58	4.45
		$^2A\ldots(33a)^2(34a)^2(35a)^2(36a)^2(37a)^2(38a)^1(39a)^2(40a)^2(41a)^2$	4.77	4.63
		$^2A\ldots(33a)^2(34a)^2(35a)^2(36a)^2(37a)^1(38a)^2(39a)^2(40a)^2(41a)^2$	5.44	5.19
		$^2A\ldots(33a)^2(34a)^2(35a)^2(36a)^1(37a)^2(38a)^2(39a)^2(40a)^2(41a)^2$	5.68	5.47
		$^2A\ldots(33a)^2(34a)^2(35a)^1(36a)^2(37a)^2(38a)^2(39a)^2(40a)^2(41a)^2$	5.96	5.72
		$^2A\ldots(33a)^2(34a)^1(35a)^2(36a)^2(37a)^2(38a)^2(39a)^2(40a)^2(41a)^2$	[d]	6.10

[a]Numbers in the parentheses represent uncertainties in the last digit.
[b]VDEs were calculated at the TD-PBE0/6-311+G* level of theory.
[c]VDEs were calculated at the TD-TPSSh/6-311+G* level of theory.
[d]This detachment channel cannot be obtained at this level of theory.

The ADE is estimated from the onset of band X as ~3.9(1) eV by drawing a straight line along the leading edge and taking the intersection with the binding energy axis plus the spectral resolution. Following a small energy gap (~0.35 eV), feature A is observed at 4.44 eV. A fairly broad feature B is observed at 4.71 eV, indicating multiple detachment channels that might contribute to this feature. Two intense features, C and D, are observed at VDEs of 5.05 eV and 5.35 eV, respectively. At the high binding energy side, features E and F are tentatively identified at 5.68 eV and 5.89 eV. An additional feature (A′)

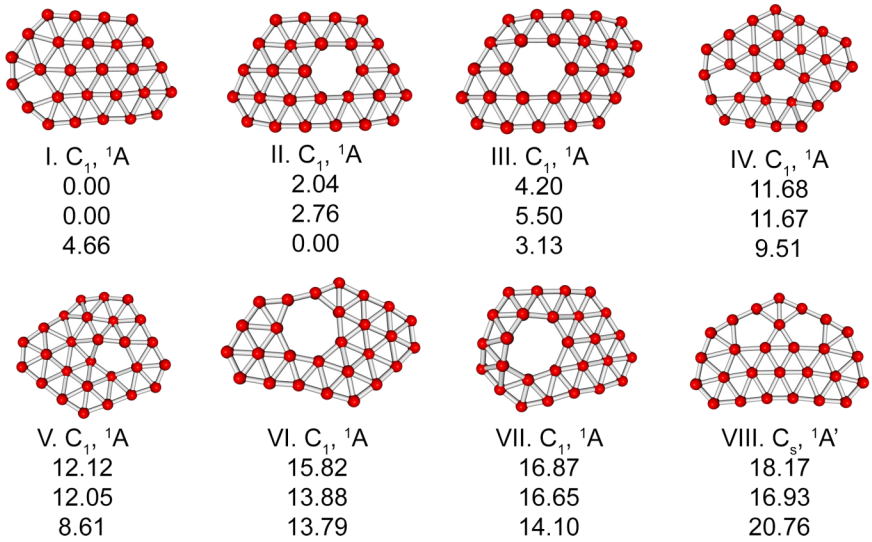

FIG. 2. Relative energies in kcal/mol of the low-lying isomers of B_{27}^- based on the PBE0/6-311+g(2df) (top), TPSSh/6-311+g(2df) (middle), and CCSD(T)/6-311-g(d) (bottom) methods. Zero-point energy corrections are included.

is identified between features A and B at a VDE of 4.56 eV. As will be discussed later, this feature A′ is likely due to a low-lying isomer of B_{27}^-.

IV. COMPUTATIONAL RESULTS

Using both the CW and BH search algorithms, we generated and optimized about 8000 trial structures, including frequency calculations. Both PBE0 and TPSSh functionals yielded more than 70 isomers within 40 kcal/mol using the 3-21g basis set. These isomers were reoptimized at DFT/6-311+G* and relative energies were calculated at DFT/6-311+G(2df) with ZPE corrections. The eight lowest lying isomers at the PBE0/6-311+g(2df) level of theory are displayed in Figure 2, where the relative energies from TPSSh and CCSD(T) are also given. The Cartesian coordinates of these isomers are given in the supplementary material.[56] Both DFT methods gave isomer **I**, a quasi-planar structure with 16 peripheral and 11 inner boron atoms, as the global minimum, but CCSD(T) gave isomer **II** as the global minimum. At the PBE0/6-311+G(2df) level, isomer **II** is only 2.04 kcal/mol above isomer **I**. The relative energy at TPSSh/6-311+G(2df) level (2.76 kcal/mol) is slightly higher than predicted by the PBE0 functional. Isomer **I** exhibits a triangular boron lattice with a slight out-of-plane distortion and a tetragonal defect. The out-of-plane distortion is quite small, only ~0.8 Å. Isomer **II** contains a hexagonal hole in a triangular lattice, which can be viewed as removing one row of three boron atoms from the top of the chiral B_{30}^- cluster.[42] Isomer **III** has a similar structural motif as isomer **II**, except that it has a different triangular lattice. Isomer **III** is 4.20 kcal/mol (PBE0), 5.50 kcal/mol (TPSSh), and 3.13 kcal/mol [CCSD(T)] above isomer **I**. All three low-lying isomers (**I**–**III**) have the same number of peripheral boron atoms (16) and interior boron atoms (11).

There is a large energy gap (~7 kcal/mol) between isomers **III** and **IV**. Four more isomers are found within 6 kcal/mol by the DFT methods and 12 kcal/mol by CCSD(T). Isomer **V** contains a pentagonal hole, whereas isomers **IV** and **VIII** contain a double pentagonal hole. Interestingly, isomers **VI** and **VII** each contain a heptagonal vacancy. There seems to be a tendency of larger vacancies with the cluster size, as suggested before.[25,40,42]

V. COMPARISON BETWEEN THEORY AND EXPERIMENT

The low-lying isomers of B_{27}^- are closed shell, and thus only doublet final states are expected upon one electron detachment. Clearly, the three lowest energy isomers are all very close in energy and the current theoretical calculations are not sufficient to determine the global minimum. Hence, comparison with the experimental data is critical to determine the true global minimum. The calculated VDEs for isomers **I** (C_1, ^1A), **II** (C_1, ^1A), and **III** (C_1, ^1A) at DFT/6-311+g* are shown in Table I, where they are compared with the experimental VDEs. Their simulated spectra are compared with the experimental data in Figure 3. Both PBE0 and TPSSh methods give similar VDEs, and thus only the PBE0 results will be used for the following discussion.

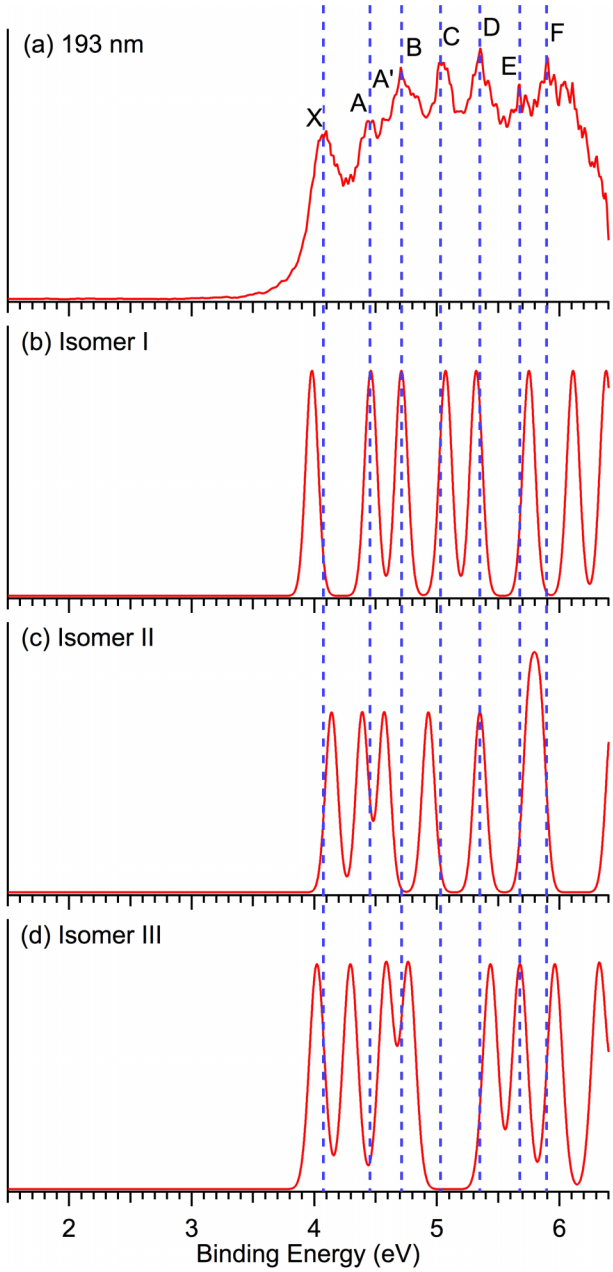

FIG. 3. Comparison between the simulated spectra for isomers **I** (b), **II** (c), and **III** (d) with the experimental spectrum (a). The simulated spectra were created by fitting Gaussian functions with a 0.26 eV full width at half height to the TD-PBE0 VDE values.

A. Isomer I

The first VDE of B_{27}^- corresponds to electron detachment from the doubly occupied HOMO (41a) to produce the neutral ^2A ground state. As shown in Table I, the first VDE calculated at PBE0 level is 3.98 eV, which is in excellent agreement with the experimental value of 4.09 eV. The next detachment channel from HOMO-1 yields a VDE at 4.46 eV, which also agrees well with band A at 4.44 eV. In fact, all the computed higher VDEs from isomer **I** are in excellent agreement with the experimental data (Table I). This good agreement can be seen more clearly from the comparison of the simulated spectrum (Figure 3(b)) with the experimental spectrum re-

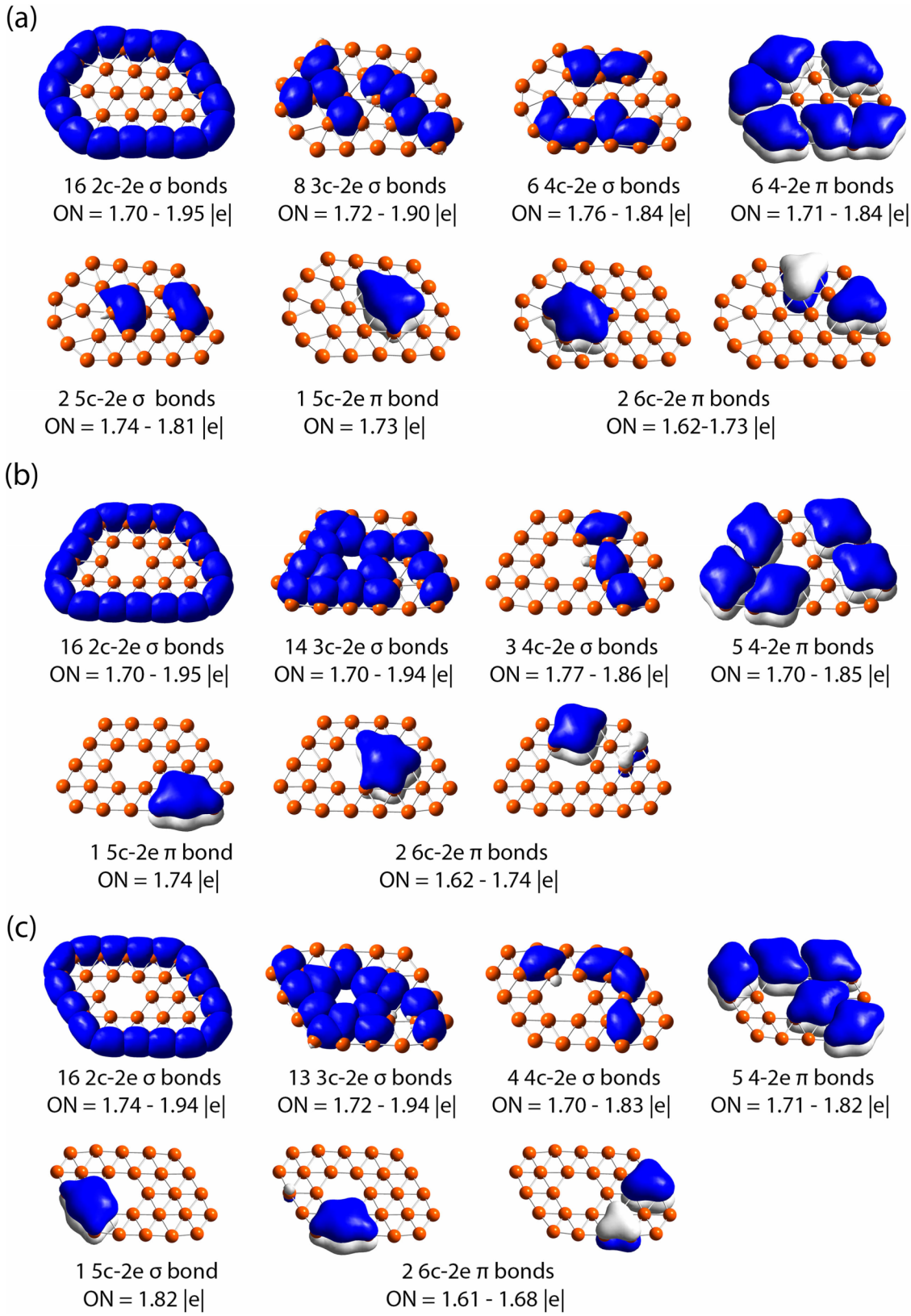

FIG. 4. AdNDP analyses of B_{27}^-: (a) for isomer **I**, (b) for isomer **II**, and (c) for isomer **III**. ON represents occupation number.

produced in Fig. 3(a). However, the A′ feature discernible between bands A and B in the experimental spectrum cannot be explained by isomer **I**, hinting at the presence of another minor isomer.

B. Isomers II and III

Isomer **II** is the global minimum at the CCSD(T) level of theory and it is only 2.04 kcal/mol (PBE0) and 2.76 kcal/mol

(TPSSh) above isomer **I**, and could co-exist in the cluster beam under our experimental conditions with isomer **I**. As shown in Table I and Figure 3(c), the first VDE of isomer **II** is predicted to be 4.14 eV, slightly above the measured VDE of band X at 4.09 eV. Because of the broad spectral width, we cannot rule out contribution of isomer **II** to band X. In fact, all other higher VDEs of isomer **II** could contribute to the width of the experimental spectrum, except the third VDE calculated at 4.57 eV, which is in excellent agreement with the observed VDE of feature A′ at 4.56 eV. This feature provides the most tangible evidence of the presence of isomer **II** experimentally.

Isomer **III** lies 4.20 kcal/mol (PBE0) and 5.50 (TPSSh) kcal/mol above isomer **I**. However, CCDD(T) suggests that isomer **III** is lower in energy than isomer **I** by 1.56 kcal/mol. The calculated VDEs from isomer **III** are also given in Table I and the simulated spectrum is presented in Figure 3(d). The overall pattern of the simulated spectrum from isomer **III** clearly disagrees with that of the experimental spectrum, although we could not completely rule out small contributions because of the broad PES bands.

VI. DISCUSSION

The excellent agreement between the theoretical VDEs and the observed PES spectrum provides considerable credence to the identification of isomer **I** as the global minimum of B_{27}^-, with isomers **II** and **III** as low-lying isomers, which might be present experimentally as minor species. In the current case, it appears that the DFT methods agree better with the experiment, whereas the usually more reliable CCSD(T) method underestimates the stability of isomer **I**. The chemical bonding analyses of isomers **I**, **II**, and **III** were carried out using AdNDP analyses,[52] as shown in Figure 4. The structures of these three isomers are not truly planar; therefore the AdNDP analyses were performed on their corresponding flattened structures to better appreciate the σ- and π-bonding.

Fig. 4(a) shows 16 classical 2c–2e σ bonds on the periphery of isomer **I**, similar to the bonding pattern observed in all the smaller boron clusters.[25] Their occupation numbers (ON) are from 1.70 |e| to 1.95 |e|, close to the ideal case of 2.00 |e|. The variation of occupation numbers of the peripheral B–B bonds is also consistent with the slightly different B–B bond lengths on the edge. The σ bonds associated with the inner boron atoms are all delocalized, including eight 3c–2e σ bonds, six 4c–2e σ bonds, and two 5c–2e σ bonds. These delocalized σ bonds cover the whole cluster plane quite evenly. The π electron density can be partitioned into three delocalized bonding sets: six 4c–2e π bonds, one 5c–2e π bond, and two 6c–2e π bonds. This π-bonding pattern is very similar to the bonding pattern of the global minimum of B_{25}^-,[14] which has eight delocalized π bonds, although B_{27}^- has one more 6c–2e π bond due to two additional boron atoms. Thus, in 2D boron clusters with triangular lattices, the ratio of valence electrons involved in *delocalized* σ and π bond is approximately 2:1.

The AdNDP results of the B_{27}^- isomer **II** are shown in the Figure 4(b). Again, there are 16 peripheral classical 2c–2e σ bonds, as observed in all 2D boron clusters. The interior σ electron density of isomer **II** can be partitioned into 14 3c–2e and three 4c–2e delocalized σ bonds. Similar to the bonding patterns in B_{30}^-, B_{35}^-, and B_{36}^- clusters,[38,39,42] the hexagonal vacancy in isomer **II** of B_{27}^- is surrounded by six 3c–2e delocalized σ bonds. Eight delocalized π bonds are observed, including five 4c–2e, one 5c–2e, and two 6c–2e π bonds (Figure 4(b)). It is interesting to note that in comparison to isomer **I**, the hexagonal vacancy in isomer **II** "converts" one delocalized π bond to a delocalized σ bond. It should also be pointed out that the ratios of the delocalized σ and π bonds for 2D boron clusters with the hexagonal vacancies are all larger than 2, including B_{30}^-, B_{35}^-, B_{36}^-, and isomer **II** of B_{27}^- (17/8 = 2.13). On the other hand, for 2D boron clusters with smaller vacancies (tetragonal or pentagonal), the ratios of the delocalized σ and π bonds are all smaller than 2, such as that in isomer **I** of B_{27}^- (16/9 = 1.78).

The AdNDP results of isomer **III** of B_{27}^- are similar to those of isomer **II**. In addition to the 16 2c–2e σ bonds localized on the periphery, we found 14 3c–2e delocalized σ bonds, three 4c–2e delcoalized σ bonds, and eight delocalized π bonds. Again, the ratio of the delocalized σ and π bond in isomer **III** is large than 2 and is the same as isomer **II**, because of the presence of the hexagonal vacancy. Thus, a major electronic effect of the hexagonal hole in 2D boron clusters is the increase of delocalized σ bonds at the expense of delocalized π bonds.

VII. CONCLUSIONS

We report a joint photoelectron spectroscopic and theoretical study on the structures and chemical bonding of the B_{27}^- cluster. Extensive global minimum searches revealed a quasi-planar structure with a tetragonal vacancy (**I**) as the global minimum and two co-existing low-lying isomers with hexagonal vacancies (**II** and **III**). Comparison between the simulated spectra and the experimental data showed that the isomer **I** is mainly responsible for the observed photoelectron spectrum, while isomers **II** and **III** are also present experimentally. Chemical bonding analyses showed that all these three isomers have 16 peripheral 2c–2e B-B σ-bonding. However, isomer **I** has 16 delocalized σ bonds and 9 delocalized π bonds, while isomers **II** and **III** have 17 delocalized σ bonds and 8 delocalized π bonds. The hexagonal vacancy seems to favor more delocalized σ bonds relative to π bonds. The global minimum isomer **I** is related to the B_{25}^- cluster by adding one boron atom to the periphery and one to an interior pentagonal vacancy. Isomer **II** can be viewed as removing one row of boron atom from the hexagon-doped B_{30}^- cluster. Thus, the B_{27}^- cluster is the turning point for the appearance of the hexagonal hole, which is characteristic of borophenes.

ACKNOWLEDGMENTS

The experimental work was supported by the National Science Foundation (Grant No. CHE-1263745 to L.S.W.). The theoretical work done at UNL was supported by ARL (Grant No. W911NF1020099) and by the University of Nebraska Holland Computing Center.

[1]A. P. Sergeeva, B. B. Averkiev, H. J. Zhai, A. I. Boldyrev, and L. S. Wang, J. Chem. Phys. **134**, 224304 (2011).

[2]W. Huang, A. P. Sergeeva, H. J. Zhai, B. B. Averkiev, L. S. Wang, and A. I. Boldyrev, Nat. Chem. **2**, 202 (2010).

[3]A. P. Sergeeva, D. Y. Zubarev, H. J. Zhai, A. I. Boldyrev, and L. S. Wang, J. Am. Chem. Soc. **130**, 7244 (2008).
[4]B. Kiran, S. Bulusu, H. J. Zhai, S. Yoo, X. C. Zeng, and L. S. Wang, Proc. Natl. Acad. Sci. U. S. A. **102**, 961 (2005).
[5]W. An, S. Bulusu, Y. Gao, and X. C. Zeng, J. Chem. Phys. **124**, 154310 (2006).
[6]A. N. Alexandrova, A. I. Boldyrev, H. J. Zhai, and L. S. Wang, J. Phys. Chem. A **108**, 3509 (2004).
[7]A. N. Alexandrova, A. I. Boldyrev, H. J. Zhai, L. S. Wang, E. Steiner, and P. W. Fowler, J. Phys. Chem. A **107**, 1359 (2003).
[8]H. J. Zhai, L. S. Wang, A. N. Alexandrova, and A. I. Boldyrev, J. Phys. Chem. A **107**, 9319 (2003).
[9]H. J. Zhai, B. Kiran, J. Li, and L. S. Wang, Nat. Mater. **2**, 827 (2003).
[10]H. J. Zhai, L. S. Wang, A. N. Alexandrova, and A. I. Boldyrev, J. Chem. Phys. **117**, 7917 (2002).
[11]I. A. Popov, Z. A. Piazza, W. L. Li, L. S. Wang, and A. I. Boldyrev, J. Chem. Phys. **139**, 144307 (2013).
[12]Z. A. Piazza, W. L. Li, C. Romanescu, A. P. Sergeeva, L. S. Wang, and A. I. Boldyrev, J. Chem. Phys. **136**, 104310 (2012).
[13]A. P. Sergeeva, Z. A. Piazza, C. Romanescu, W. L. Li, A. I. Boldyrev, and L. S. Wang, J. Am. Chem. Soc. **134**, 18065 (2012).
[14]Z. A. Piazza, I. A. Popov, W. L. Li, R. Pal, X. C. Zeng, A. I. Boldyrev, and L. S. Wang, J. Chem. Phys. **141**, 034303 (2014).
[15]N. Vast, S. Baroni, G. Zerah, J. M. Besson, A. Polian, M. Grimsditch, and J. C. Chervin, Phys. Rev. Lett. **78**, 693 (1997).
[16]M. Fujimori, T. Nakata, T. Nakayama, E. Nishibori, K. Kimura, M. Takata, and M. Sakata, Phys. Rev. Lett. **82**, 4452 (1999).
[17]B. Albert and H. Hillebrecht, Angew. Chem., Int. Ed. **48**, 8640 (2009).
[18]E. Oger, N. R. M. Crawford, R. Kelting, P. Weis, M. M. Kappes, and R. Ahlrichs, Angew. Chem., Int. Ed. **46**, 8503 (2007).
[19]C. Romanescu, D. J. Harding, A. Fielicke, and L. S. Wang, J. Chem. Phys. **137**, 014317 (2012).
[20]J. O. C. Jiménez-Halla, R. Islas, T. Heine, and G. Merino, Angew. Chem., Int. Ed. **49**, 5668 (2010).
[21]G. Martínez-Guajardo, A. P. Sergeeva, A. I. Boldyrev, T. Heine, J. M. Ugalde, and G. Merino, Chem. Commun. **47**, 6242 (2011).
[22]J. Zhang, A. P. Sergeeva, M. Sparta, and A. N. Alexandrova, Angew. Chem., Int. Ed. **51**, 8512 (2012).
[23]G. Merino and T. Heine, Angew. Chem., Int. Ed. **51**, 10226 (2012).
[24]D. Moreno, S. Pan, L. L. Zeonjuk, R. Islas, E. Osorio, G. Martínez-Guajardo, P. K. Chattaraj, T. Heine, and G. Merino, Chem. Commun. **50**, 8140 (2014).
[25]A. P. Sergeeva, I. A. Popov, Z. A. Piazza, W. L. Li, C. Romanescu, L. S. Wang, and A. I. Boldyrev, Acc. Chem. Res. **47**, 1349 (2014).
[26]I. Boustani, A. Quandt, E. Hernandez, and A. Rubio, J. Chem. Phys. **110**, 3176 (1999).
[27]M. H. Evans, J. D. Joannopoulos, and S. T. Pantelides, Phys. Rev. B **72**, 045434 (2005).
[28]J. Kunstmann and A. Quandt, Phys. Rev. B **74**, 035413 (2006).
[29]K. C. Lau and R. Pandey, J. Phys. Chem. C **111**, 2906 (2007).
[30]I. Cabria, J. A. Alonso, and M. J. López, Phys. Status Solidi A **203**, 1105 (2006).
[31]H. Tang and S. Ismail-Beigi, Phys. Rev. Lett. **99**, 115501 (2007).
[32]X. B. Yang, Y. Ding, and J. Ni, Phys. Rev. B **77**, 041402R (2008).
[33]L. A. Chernozatonskii, P. B. Sorokin, and B. I. Yakobson, JETP Lett. **87**, 489 (2008).
[34]Y. Ding, X. Yang, and J. Ni, Appl. Phys. Lett. **93**, 043107 (2008).
[35]H. Tang and S. Ismail-Beigi, Phys. Rev. B **82**, 134113 (2010).
[36]E. S. Penev, S. Bhowmick, A. Sadrzadeh, and B. Yakobson, Nano Lett. **12**, 2441 (2012).
[37]X. J. Wu, J. Dai, Y. Zhao, Z. Zhuo, J. L. Yang, and X. C. Zeng, ACS Nano **6**, 7443 (2012).
[38]Z. A. Piazza, H. S. Hu, W. L. Li, Y. F. Zhao, J. Li, and L. S. Wang, Nat. Commun. **5**, 3113 (2014).
[39]W. L. Li, Q. Chen, W. J. Tian, H. Bai, Y. F. Zhao, H. S. Hu, J. Li, H. J. Zhai, S. D. Li, and L. S. Wang, J. Am. Chem. Soc. **136**, 12257 (2014).
[40]H. J. Zhai, Y. F. Zhao, W. L. Li, Q. Chen, H. Bai, H. S. Hu, Z. A. Piazza, W. J. Tian, H. G. Lu, Y. B. Wu, Y. W. Mu, G. F. Wei, Z. P. Liu, J. Li, S. D. Li, and L. S. Wang, Nat. Chem. **6**, 727 (2014).
[41]Q. Chen, W. L. Li, Y. F. Zhao, S. Y. Zhang, H. S. Hu, H. Bai, H. R. Li, W. J. Tian, H. G. Lu, H. J. Zhai, S. D. Li, J. Li, and L. S. Wang, ACS Nano **9**, 754 (2015).
[42]W. L. Li, Y. F. Zhao, H. S. Hu, J. Li, and L. S. Wang, Angew. Chem., Int. Ed. **53**, 5540 (2014).
[43]L. S. Wang, H. S. Cheng, and J. W. Fan, J. Chem. Phys. **102**, 9480 (1995).
[44]J. Akola, M. Manninen, H. Hakkinen, U. Landman, X. Li, and L. S. Wang, Phys. Rev. B **60**, R11297 (1999).
[45]W. Huang and L. S. Wang, Phys. Rev. Lett. **102**, 153401 (2009).
[46]D. J. Wales and J. P. K. Doye, J. Phys. Chem. A **101**, 5111 (1997).
[47]C. Adamo and V. Barone, J. Chem. Phys. **110**, 6158 (1999).
[48]J. P. Perdew, K. Burke, and M. Ernzerhof, Phys. Rev. Lett. **77**, 3865 (1996).
[49]J. Tao, J. P. Perdew, V. N. Staroverov, and G. E. Scuseria, Phys. Rev. Lett. **91**, 146401 (2003).
[50]M. S. Gordon, J. S. Binkley, J. A. Pople, W. J. Pietro, and W. J. Hehre, J. Am. Chem. Soc. **104**, 2797 (1982).
[51]T. Clark, J. Chandrasekhar, G. W. Spitznagel, and P. V. R. Schleyer, J. Comput. Chem. **4**, 294 (1983).
[52]D. Y. Zubarev and A. I. Boldyrev, Phys. Chem. Chem. Phys. **10**, 5207 (2008).
[53]M. J. Frisch *et al.*, GAUSSIAN 09, Revision D.01, Gaussian, Inc., Wallingford, CT, 2009.
[54]U. Varetto, Molekel 5.4.0.8, Swiss National Supercomputing Centre, Manno, Switzerland, 2009.
[55]T. Dennington, T. Keith, and J. Millam, Shawnee Mission, KS, Semichem, Inc., 2007.
[56]See supplementary material at http://dx.doi.org/10.1063/1.4921732 for the coordinates of the lowest 8 isomers.